International Journal of Microwave and Wireless Technologies

cambridge.org/mrf

Wideband isolation-improved substrate-integrated waveguide power dividers/combiners

Yong Mao Huang[1], Haiyan Jin[2], Yuliang Zhou[2], Supeng Leng[2] and Maurizio Bozzi[3]

[1]School of Electrical and Electronic Information, Xihua University, Chengdu 600039, China; [2]School of Communication and Information Engineering, University of Electronic Science and Technology of China, Chengdu 611731, China and [3]Department of Electrical, Computer, and Biomedical Engineering, University of Pavia, 27100 Pavia, Italy

Research Paper

Cite this article: Huang YM, Jin H, Zhou Y, Leng S, Bozzi M (2018). Wideband isolation-improved substrate-integrated waveguide power dividers/combiners. *International Journal of Microwave and Wireless Technologies* **10**, 1019–1027. https://doi.org/10.1017/S1759078718000995

Received: 29 August 2017
Revised: 25 May 2018
Accepted: 29 May 2018
First published online: 4 October 2018

Key words:
Filters; passive components and circuits

Author for correspondence:
Yong Mao Huang,
E-mail: ymhuang128@gmail.com

Abstract

In this paper, a 3 dB *H*-plane substrate-integrated waveguide (SIW) power divider/combiner with improved isolation is reported. By adding two isolated ports into the Y-junction, it will perform like a multi-port coupler, so that the isolation between its dividing ports can be effectively improved as the newly-added ports are properly matched. To verify the availability and effectiveness of this concept, two prototypes, one is terminated by coaxial terminations and the other is loaded with lumped resistors, are developed. Their measured results are separately in good agreement with their corresponding simulations. Meanwhile, isolations better than 16 dB with fractional bandwidth (FBW) of 35 and 25% are achieved, respectively, as well as low phase and amplitude imbalances. Compared with some reported similar SIW power dividers, the proposed ones exhibit wider FBW with similar isolation, insertion loss, phase, and amplitude balance performance.

Introduction

Substrate-integrated waveguide (SIW) integrates the characteristics of the uniplanar rectangular waveguide (RWG) and planar transmission lines, which establish an attractive trade-off between them [1]. During the past few years, a lot of microwave components and circuits have been realized in SIW technology, among which SIW power dividers with high isolation and broad bandwidth have attracted unique attention since they are highly desired in power-combining amplifiers and phased array antennas [2–6]. In [2], a half-mode SIW (HMSIW) power divider with transverse electric – 20 (TE_{20}) mode suppression achieved isolation over 10 dB with an operation frequency range of 18–35 GHz. However, its isolation is still not good enough and will be limited by the strong parasitic effect of the lumped resistor at a higher frequency. To overcome these drawbacks, another HMSIW power divider soldered the isolated resistor on the spacing slot between the two HMSIW branches [3]. It achieves isolation over 15 dB from 9.5 to 13.5 GHz, corresponding to fractional bandwidth (FBW) of 35%. However, its isolation and output return loss swings with the value and location variations of the isolated resistor, which causes extra complexity. In [4], an eight-way power splitter with over 65% FBW is implemented by utilizing the ridge SIW. However, its T-junction building block has no isolation inherently. A six-port power-dividing network shows the isolation of 20 dB over 12–16 GHz [5]. Unfortunately, its phase imbalance can exceed 10° in several frequency ranges, and insertion loss at edges of its pass-band rolls off rapidly. Recently, a multilayer SIW power divider with embedded thick film resistive septum exhibits over 22 dB isolation over 18.5–22 GHz [6]. Another SIW power divider integrated with thick film resistive layer even shows 40% FBW with 20 dB isolation [7]. Nevertheless, their realization requires a costly and complex thick film fabrication process.

On the other hand, based on the similarity of their structures, the classical RWG works can provide promising ideas for the investigation of SIW technology. For instance, a six-port building block for power distribution and combination is proposed based on the Riblet coupler [8, 9]. Moreover, a modified five-port two-way RWG power divider with equal-ratio in in-phase power distribution operation has been developed in [10]. Its SIW version incorporating absorbing material for impedance matching has even been briefly reported in [11]. However, both [10, 11] just shortly present their corresponding works, whereas none of them focused on the detailed theoretical analyses of this five-port power dividing/combining unit cell, which is inconvenient and incomprehensive for its further applications to other microwave components and circuits. In this paper, two wideband well-balanced SIW power dividers/combiners employing the five-port unit cell were used as reported in [10]. Section "SIW power dividing/combining unit cell" detailed explains the basic transmission property of the five-port power combining/dividing unit cell with both theoretical analyses and

© Cambridge University Press and the European Microwave Association 2018

CAMBRIDGE UNIVERSITY PRESS

numerical simulations. Subsequently, the design procedures of the prototypes and discussions on the experimental results are successively shown in Section "Experimental results". Finally, a conclusion is given.

SIW power dividing/combining unit cell

Figure 1 sketches signal flows in the conventional Y-junction and the five-port power dividing/combining unit cell, in which the solid arrows denote power dividing operation and the dash arrows denote power combining operation. For the conventional Y-junction, the power dividing operation can achieve small reflection but bad isolation, while the power combining operation exhibits large reflection inherently, resulting in its unavailability for practical applications. However, for the five-port power dividing/combining unit cell, its operation principles will be much different owing to the influence from the two newly-added ports.

First of all, the basic properties of the five-port power dividing/combining unit cell are investigated on the basis of the microwave network theory. As is known, the scattering matrix of an arbitrary five-port unit cell can be expressed as

$$[S] = \begin{bmatrix} S_{11} & S_{12} & S_{13} & S_{14} & S_{15} \\ S_{21} & S_{22} & S_{23} & S_{24} & S_{25} \\ S_{31} & S_{32} & S_{33} & S_{34} & S_{35} \\ S_{41} & S_{42} & S_{43} & S_{44} & S_{45} \\ S_{51} & S_{52} & S_{53} & S_{54} & S_{55} \end{bmatrix}. \quad (1)$$

If the five-port unit cell is passive and contains no anisotropic material, then it must be reciprocal and its scattering matrix will be symmetrical. In other words, $S_{ij} = S_{ji}$, and $i \neq j$. And, if all the five ports are matched, then $S_{ii} = 0$. So the scattering matrix will be as follows:

$$[S] = \begin{bmatrix} 0 & S_{12} & S_{13} & S_{14} & S_{15} \\ S_{12} & 0 & S_{23} & S_{24} & S_{25} \\ S_{13} & S_{23} & 0 & S_{34} & S_{35} \\ S_{14} & S_{24} & S_{34} & 0 & S_{45} \\ S_{15} & S_{25} & S_{35} & S_{45} & 0 \end{bmatrix}. \quad (2)$$

Subsequently, as shown in Fig. 1, the five-port power dividing/combining unit cell is longitudinally axisymmetric along the center-line of port P1. That is, ports P2 and P4 are, respectively, symmetrical with P3 and P5. Then, $S_{12} = S_{13}$, $S_{14} = S_{15}$, $S_{24} = S_{35}$, $S_{34} = S_{25}$, and $S_{24} \neq S_{25}$, $S_{34} \neq S_{35}$. Hence, the scattering matrix is simplified as follows:

$$[S] = \begin{bmatrix} 0 & S_{12} & S_{12} & S_{14} & S_{14} \\ S_{12} & 0 & S_{23} & S_{24} & S_{25} \\ S_{12} & S_{23} & 0 & S_{25} & S_{24} \\ S_{14} & S_{24} & S_{25} & 0 & S_{45} \\ S_{14} & S_{25} & S_{24} & S_{45} & 0 \end{bmatrix}. \quad (3)$$

Moreover, if the five-port unit cell is lossless, then ten independent equations can be obtained under the unitarity condition as

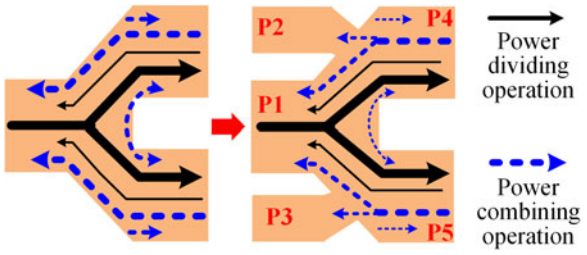


Fig. 1. Signal flows in the five-port power dividing/combining unit cell.

below [12, 13]:

$$\begin{cases} S_{12}S_{12}^* + S_{12}S_{12}^* + S_{14}S_{14}^* + S_{14}S_{14}^* = 1, \\ S_{12}S_{12}^* + S_{23}S_{23}^* + S_{24}S_{24}^* + S_{25}S_{25}^* = 1, \\ S_{14}S_{14}^* + S_{24}S_{24}^* + S_{25}S_{25}^* + S_{45}S_{45}^* = 1, \\ S_{12}S_{23}^* + S_{14}S_{24}^* + S_{14}S_{25}^* = 0, \\ S_{12}S_{24}^* + S_{12}S_{25}^* + S_{14}S_{45}^* = 0, \\ S_{12}S_{12}^* + S_{24}S_{25}^* + S_{25}S_{24}^* = 0, \\ S_{12}S_{14}^* + S_{23}S_{25}^* + S_{25}S_{45}^* = 0, \\ S_{12}S_{14}^* + S_{23}S_{25}^* + S_{24}S_{45}^* = 0, \\ S_{12}S_{14}^* + S_{23}S_{24}^* + S_{24}S_{45}^* = 0, \\ S_{14}S_{14}^* + S_{24}S_{25}^* + S_{25}S_{24}^* = 0. \end{cases} \quad (4)$$

Then, by using the similar calculation processes introduced in [13], the ideal unitary scattering matrix of the five-port power dividing/combining unit cell is given as

$$[S] = \frac{1}{2}\begin{bmatrix} 0 & 0 & 0 & \sqrt{2} & \sqrt{2} \\ 0 & 0 & \sqrt{2} & 1 & j \\ 0 & \sqrt{2} & 0 & j & 1 \\ \sqrt{2} & 1 & j & 0 & 0 \\ \sqrt{2} & j & 1 & 0 & 0 \end{bmatrix}. \quad (5)$$

According to (5), as the signal inputs the five-port unit cell from port P1, ports P4 and P5 will receive equal power while no output can be received at ports P2 and P3. Meanwhile, ports P4 and P4 are isolated. Therefore, the five-port unit cell can be utilized to develop a highly isolated two-way power divider/combiner.

Meanwhile, it has been well known that the physical sizes of SIW components and circuits are much more compact than their corresponding RWG counterparts, which are mainly due to the planarization of their structure and the increasing permittivity of their substrates. Hence, to extend the availability and practicability of the five-port unit cell in microwave systems, especially in the system integration and packaging, the SIW technology is selected as the implementation platform.

Figure 2 shows the geometry and equivalent-circuit models of the five-port SIW dividing/combining unit cell, which can be further studied by using the even–odd mode analysis method. In Fig. 2(a), the area between cross-sections XX' and YY' denotes the coupling region, with width wc and length lc, respectively. According to Fig. 2(b), once Ports P4 and P5 are driven by in-phase signals, the five-port SIW unit cell is under even–mode operation and its longitudinal symmetrical line can be equivalent as the magnetic wall. With the structure symmetry, as the in-phase waves of the TE_{10} mode in P4 and P5 propagate in the coupling region, only the even-distributed modes such as TE_{10}, TE_{30}, and TE_{50} modes can be excited. And after propagating through XX'', the higher-order TE_{30} and TE_{50} modes will be

https://doi.org/10.1017/S1759078718000995 Published online by Cambridge University Press

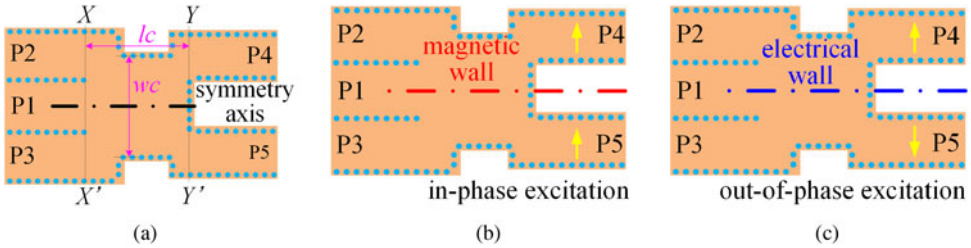


Fig. 2. (a) Geometry, (b) even-mode equivalent-circuit model, and (c) odd-mode equivalent-circuit model of the five-port SIW power dividing/combining unit cell.

cutoff whereas only the TE_{10} mode can be supported. Meanwhile, the remained signals will remain in-phase so that to add up with each other at P1 but are out-of-phase and consequently subtracted at P2 and P3. On the other hand, for the odd-mode case in Fig. 2(c), as two out-of-phase signals input the unit cell from P4 and P5 separately, the longitudinal symmetrical line will perform like the electrical wall. Therefore, as the out-of-phase waves of TE_{10} mode propagate in the coupling region, they will excite the odd-distributed TE_{20} and TE_{40} modes, which will be cut-off after crossing over XX'. Due to the influence of the electrical wall, port P1 will be cut into two narrower waveguides so that all modes will be cutoff. Hence, no output can be captured at P1. On the contrary, signals coming from P4 and P5 will be fed into P2 and P3. Additionally, as a signal inputs the five-port SIW unit cell from P1, only the even-distributed TE_{10}, TE_{30} and TE_{50} modes can be excited in the coupling region, which can be deduced from the reciprocity of the unit cell, or inferred from its structure symmetry. In a word, the five-port SIW unit cell can act as a two-way in-phase power divider/combiner. Meanwhile, it will also be useful in the separation of the differential- and common-mode coefficients of signals.

Afterwards, it is important to discuss the size determination of the five-port SIW unit cell. Firstly, widths of the five ports are mainly determined by the operation frequency range. Generally, the cutoff frequency of the dominant mode determined by the SIW width is supposed to be lower than the lowest operation frequency. Based on the operation frequency range, widths of the five SIW ports can be selected rapidly. Secondly, the width of the coupling region, *wc*, is mainly determined by the number of transmissible modes in the coupling region. Typically, only the single TE_{10} mode or TE_{10}/TE_{30} modes are suitable for low-loss transmission. Based on the SIW theory, the cut-off wavelengths of TE_{10}, TE_{30} and TE_{50} modes are as follows:

$$\begin{aligned} \lambda_{c\text{-}10} &= 2\pi/k_{c\text{-}10} = 2a_{SIW}, \\ \lambda_{c\text{-}30} &= 2\pi/k_{c\text{-}30} = 2a_{SIW}/3, \\ \lambda_{c\text{-}50} &= 2\pi/k_{c\text{-}50} = 2a_{SIW}/5. \end{aligned} \tag{6}$$

where a_{SIW} is the equivalent width of SIW and can be calculated by $a_{SIW} = a - 4.32R^2/p + 0.4R^2/a$, in which R is the radius of metallic vias and p is the center-to-center spacing of adjacent vias.

If only TE_{10} mode is transmissible in the coupling region, the guided wavelength λ_g should satisfy:

$$\lambda_{c\text{-}30} < \lambda_g < \lambda_{c\text{-}10} \Rightarrow 0.5\lambda_g < a_{SIW} < 1.5\lambda_g. \tag{7}$$

If both TE10 and TE30 modes are supported in the coupling region, it can be obtained that

$$\lambda_{c\text{-}50} < \lambda_g < \lambda_{c\text{-}30} \Rightarrow 1.5\lambda_g < a_{SIW} < 2.5\lambda_g. \tag{8}$$

Therefore, once the permitted modes in the coupling region are selected, *a* can be determined.

Thirdly, length of the coupling region, *lc*, is also mainly determined by the number of permitted modes in it. If only the TE_{10} mode is permitted in the coupling region, its electric (E)-field magnitude in the middle is much stronger than that at both edges. After propagating from XX'' to YY'', the E-field magnitude of the TE_{10} mode around the metallic vias in the middle of YY'' is still much stronger than that at both edges, which consequently causes strong input reflection. Hence, only supporting the TE_{10} mode in the coupling region can achieve short *lc*, but also result in bad input return loss. On the other hand, if both TE_{10} and TE_{30} modes are transmissible, the situation will be much different. As depicted in [10, 11], after propagating through the same length *lc*, TE_{10} and TE_{30} modes are with electrical lengths of θ_{10} and θ_{30}, which are given as

$$\theta_{10} = \beta_{10} \cdot lc, \quad \theta_{30} = \beta_{30} \cdot lc, \tag{9}$$

where β_{10} and β_{30} are the phase constants of TE_{10} and TE_{30} modes, respectively.

As TE_{10} and TE_{30} modes arrive at YY', they are supposed to be out-of-phase in the middle but in-phase at both edges. Being out-of-phase in the middle means the two modes will subtract, thus decreasing the strength of the E-field near the metallic vias in the middle and ultimately decreasing the input reflection. Meanwhile, being in-phase at both edges will make the TE_{10} and TE_{30} modes add up together so that more electromagnetic (EM) energy can be fed into the dividing ports. Hence, transmission with both TE_{10} and TE_{30} modes in the coupling region is better than that with the single TE_{10} mode. To perform such an operation, θ_{10}–θ_{30} should satisfy

$$\theta_{10} - \theta_{30} = 2(n-1)\pi, \tag{10}$$

where n is a positive integer. Then, *lc* is calculated as

$$lc = (2n-1)\pi/(\beta_{10} - \beta_{30}) = \pi/(\beta_{10} - \beta_{30}). \tag{11}$$

Here n is set as 1 for size reduction.

Furthermore, it is necessary to realize that the above calculations are in allusion to single frequency operation. In order to avoid the steep and acute change of wave propagation caused by the discontinuities in the five-port SIW unit cell, some matching structures and transitions are essential to be employed to

https://doi.org/10.1017/S1759078718000995 Published online by Cambridge University Press

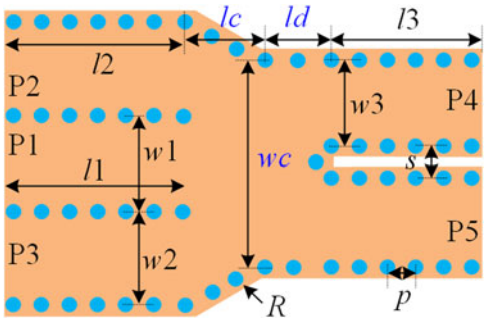


Fig. 3. Geometry of the five-port SIW power dividing/combining unit cell with taper-shaped transition structure.

improve the impedance matching performance, so that to broaden the operation bandwidth. Therefore, the taper-shaped SIW structure is introduced into the five-port SIW power dividing/combining unit cell, and the modified geometry is illustrated in Fig. 3.

Thereafter, to demonstrate the aforementioned theoretical analyses, some full wave EM simulations are carried out on the five-port SIW power dividing/combining unit cell by using the commercial finite-element-method-based simulator. In all simulations, the substrate is set with a thickness of 0.508 mm, relative permittivity of 2.94, and dielectric loss tangent of 0.0012. The copper metal is selected as the surface conductor, with a thickness of 0.035 mm. Moreover, geometrical parameters corresponding to Fig. 3 are $l1 = l2 = l3$ 10, $w1 = w2 = w3 = 8$, $lc = 6$, $wc = 18$, $s = 2$, $p = 0.8$, $R = 0.2$ (unit: mm). Figure 4 shows the simulated E-field distributions of the five-port SIW unit cell at 16 GHz under various excitations. According to Fig. 4(a), as the five-port SIW unit cell is excited from P1, most of the EM energy will propagate through the coupling region and into P4 and P5 eventually, whereas only little EM energy propagates to P2 and P3. So the unit cell can be utilized as a two-way power divider, and P1 and P2/P3 are well-isolated as well. Subsequently, as shown in Fig. 4(b), once a signal inputs the unit cell from P5, ports P1, P2, and P3 will receive signal with various strengths. Meanwhile, seldom signal energy can be captured at P4, which means good isolation between P4 and P5. Thirdly, as the unit cell is simultaneously excited with in-phase signals at P4 and P5, P1 will get much stronger EM energy, while little EM energy can be obtained at P2 and P3, as depicted in Fig. 4(c). That is to say, the unit cell can act as an in-phase power combiner. Finally, from Fig. 4(d), with simultaneously out-of-phase inputs from P4 and P5, almost all of the EM energy propagates through P2 and P3, whereas nearly no signal can be detected at P1. Hence, it can be predicted from Figs 4(c) and 4(d) that the five-port SIW unit cell can be utilized to separate the differential- and common-mode coefficients of signals.

Particularly, as sketched in Figs 4(a) and 4(c), there is still some leakage at P2 and P3, which can cause extra insertion loss in even mode. Hence, the total insertion loss of the five-port SIW power dividing/combining unit cell will consequently increase. To verify this prediction, powers of the output, the loss and leakage are investigated. Here, the output means the sum value of P4 and P5. The loss contains the dielectric loss, conductivity loss, and radiation loss, while the leakage only means output power obtained at the two isolated ports. Consider the original input power at P1 is 1, then it can be further captured from the full-wave simulation that the power relationship at 16 GHz

$$P_i{:}P_o{:}P_{loss}{:}P_{leak} = 1{:}0.91{:}0.055{:}0.035, \tag{12}$$

where P_i, P_o, P_{loss}, and P_{leak} denote input, output, loss and leakage powers, respectively.

It can be obtained from (12) that P_{leak} is comparable with P_{loss}, which means the leakage at isolated ports P2 and P3 can introduce extra loss to the whole unit cell. To overcome this issue, the size of the coupling region should be tuned carefully for the specific frequency. The taper transition can be modified slightly to keep low leakage and broadband simultaneously as well.

Finally, to illustrate the contribution from the newly-added ports visually, Fig. 5 shows the simulated isolations and output return losses of the Y-junction and the five-port SIW power dividing/combining unit cell. As shown in Fig. 5, both isolation and output return loss of the five-port SIW unit cell have been improved a lot as compared with the Y-junction. Obviously, by introducing the two isolated ports into the Y-junction, both the isolation and output return loss are enhanced effectively with the utilization of the two extra isolated ports.

In addition, it is worth mentioning that design processes of the five-port SIW power dividing/combining unit cell is simpler than those of the corresponding RWG counterpart. As depicted in [1, 2], SIW only supports TE_{m0} modes, for instance, the TE_{10}, TE_{20} and TE_{30} modes. Based on equations (6)–(11) listed above, it is quite easy to control the existence of these three modes in practical designs. However, in RWG, both TE and transverse magnetic (TM) modes can be supported. Obviously, controlling the existence of TE and TM modes in RWG is much more complex and difficult than controlling the TE_{m0} modes in SIW. Therefore, as the five-port power dividing/combining unit cell is implemented in SIW, its design processes can be much simpler and more efficient. Furthermore, for an SIW with an equivalent width of a_{SIW}, cutoff frequencies of the TE_{10} and TE_{20} modes in it are

$$f_{c\text{-}10} = \frac{1}{2\sqrt{\mu\varepsilon}} \cdot \sqrt{\left(\frac{1}{a_{SIW}}\right)^2 + \left(\frac{0}{h}\right)^2} = \frac{1}{2a_{SIW}\sqrt{\mu_r\mu_0\varepsilon_r\varepsilon_0}}, \tag{13}$$

$$f_{c\text{-}20} = \frac{1}{2\sqrt{\mu\varepsilon}} \cdot \sqrt{\left(\frac{2}{a_{SIW}}\right)^2 + \left(\frac{0}{h}\right)^2} = \frac{1}{a_{SIW}\sqrt{\mu_r\mu_0\varepsilon_r\varepsilon_0}}, \tag{14}$$

where μ_0 and ε_0 are the permeability and permittivity in free space, μ_r and ε_r are the relative permeability and permittivity of the substrate in SIW, and h represents the substrate thickness.

From (13) and (14), $2{\cdot}f_{c\text{-}10} = f_{c\text{-}20}$, then the single mode operation bandwidth in SIW is

$$BW_{SIW} = f_{c\text{-}10} - f_{c\text{-}20} = \frac{1}{2a_{SIW}\sqrt{\mu_r\mu_0\varepsilon_r\varepsilon_0}}. \tag{15}$$

For an RWG with inter cross-section size of $a \times b$ ($a > b$), cutoff frequencies of the TE_{10}, TE_{01}, and TE_{20} modes in it are

$$f_{cs\text{-}10} = \frac{1}{2\sqrt{\mu\varepsilon}} \cdot \sqrt{\left(\frac{1}{a}\right)^2 + \left(\frac{0}{b}\right)^2} = \frac{1}{2a\sqrt{\mu_0\varepsilon_0}}, \tag{16}$$

https://doi.org/10.1017/S1759078718000995 Published online by Cambridge University Press

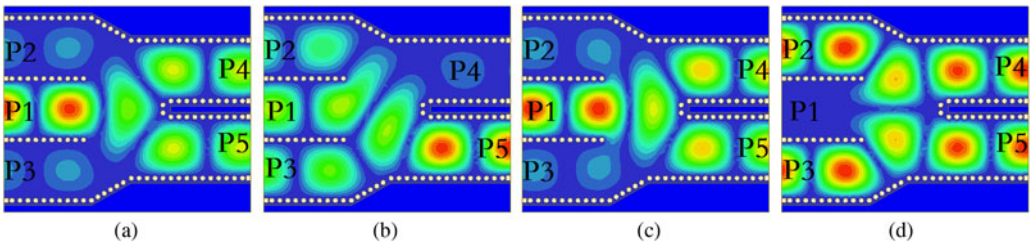


Fig. 4. E-field distribution of the unit cell in Fig. 3 at 16 GHz under various excitations. (a) Excitation from P1, (b) excitation from P5, (c) simultaneously in-phase excitation from P4 and P5, and (d) simultaneously out-of-phase excitation from P4 and P5.

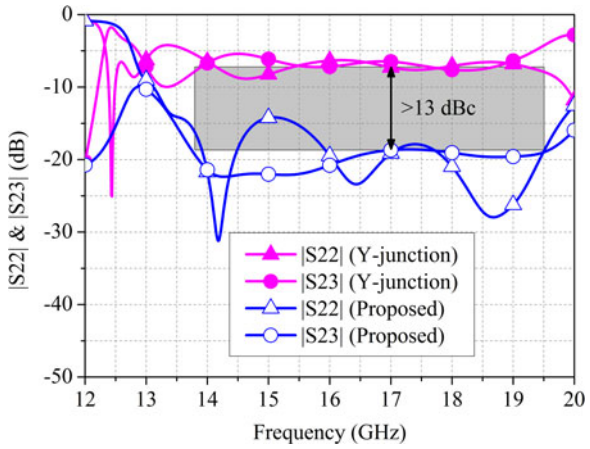


Fig. 5. Simulated isolations and output return losses of the conventional SIW Y-junction and the derived five-port SIW power combining/dividing unit cell.

$$f_{cs\text{-}01} = \frac{1}{2\sqrt{\mu\varepsilon}} \cdot \sqrt{\left(\frac{0}{a}\right)^2 + \left(\frac{1}{b}\right)^2} = \frac{1}{2b\sqrt{\mu_0\varepsilon_0}}, \tag{17}$$

$$f_{cs\text{-}20} = \frac{1}{2\sqrt{\mu\varepsilon}} \cdot \sqrt{\left(\frac{2}{a}\right)^2 + \left(\frac{0}{b}\right)^2} = \frac{1}{a\sqrt{\mu_0\varepsilon_0}}. \tag{18}$$

According to (16)–(18), $2 \cdot f_{cs\text{-}10} = f_{cs\text{-}20}$, then the single mode operation bandwidth in RWG is

$$BW_{RWG} = \begin{cases} f_{c\text{-}20} - f_{c\text{-}10} = \dfrac{1}{2a\sqrt{\mu_0\varepsilon_0}}, & a > 2b, \\ f_{c\text{-}01} - f_{c\text{-}10} = \dfrac{1}{2\sqrt{\mu_0\varepsilon_0}}\left(\dfrac{1}{b} - \dfrac{1}{a}\right), & a < 2b. \end{cases} \tag{19}$$

As SIW and RWG are with the same dominant cutoff frequency, i.e. $f_{c\text{-}10} = f_{cs\text{-}10}$, then $f_{c\text{-}20} = f_{cs\text{-}20}$. Considering these conditions with (15) and (19) together, it can be obtained that $BW_{RWG} \leq BW_{SIW}$, so the single mode operation bandwidth of RWG is no larger than that of SIW.

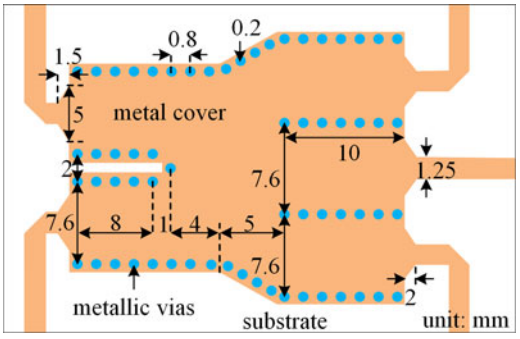


Fig. 6. Detailed configuration and optimized dimensions of the SIW power divider/combiner with coaxial terminations.

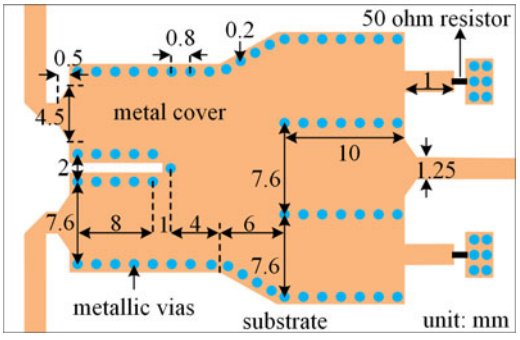


Fig. 7. Detailed configuration and optimized dimensions of the SIW power divider/combiner with lumped resistors.

Experimental results

SIW power divider/combiner with coaxial terminations

For an experimental proof of the aforementioned analysis, a 3 dB power divider/combiner prototype is designed. A detailed configuration of the SIW power combiner/divider is shown in Fig. 3. A Rogers RT/duroid 6002 substrate with a dielectric constant of 2.94 ± 0.04, loss tangent of 0.0013, thickness of 0.508 mm, and conductor thickness of 0.035 mm is used for design. Width and length of the coupling region, as well as the width of the five ports, are set up based on the conditions mentioned in Section "SIW power dividing/combining unit cell". Subsequently, five taper transitions, with different widths and lengths, are also added between the 50 Ω microstrip lines and SIW ports to achieve optimized standing-wave performance at each port, respectively. Finally, the overall structure with SubMiniature version A (SMA) connectors is modeled and simulated by using the same

https://doi.org/10.1017/S1759078718000995 Published online by Cambridge University Press

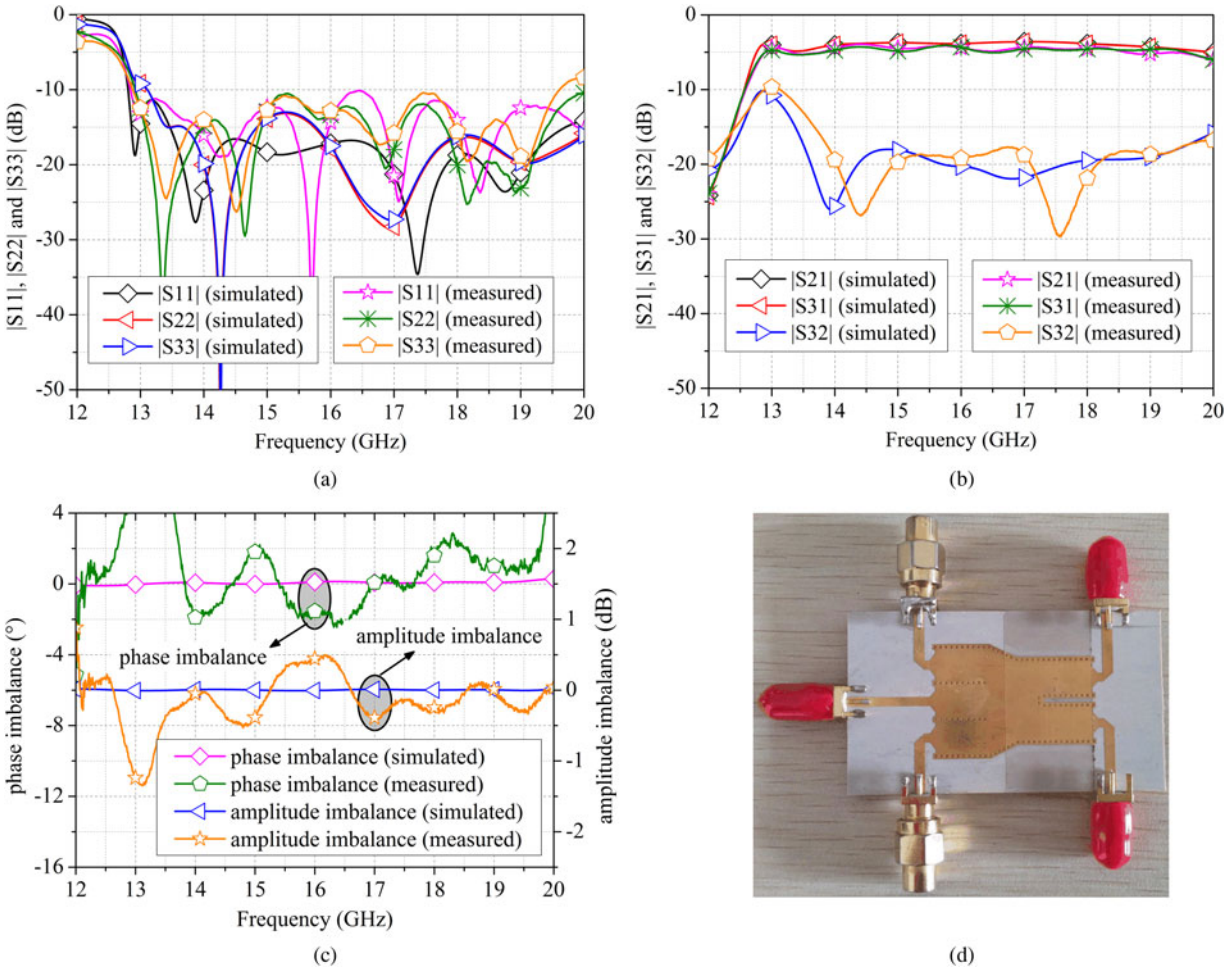


Fig. 8. Simulated and measured results of the fabricated SIW power divider/combiner with coaxial terminations. (a) Input and output return losses; (b) insertion losses and isolation; (c) phase and amplitude imbalances; (d) photograph of the fabricated prototype.

commercial full-wave simulation software mentioned above. The optimized dimensions are listed in Fig. 6 as well.

SIW power divider/combiner with lumped resistors

Thereafter, since the SIW power divider/combiner with coaxial termination is inconvenient for the printed circuit board (PCB)-level integration with other planar circuits, another experiment is done to remove the coaxial terminations by the 50 Ω lumped resistors. Most of the design procedures are exactly same as those in the coaxial one. Particularly, a 50 Ω microstrip line is connected between the isolated port and the lumped resistor, with several vias placed at the other port of lumped resistors for grounding. Afterwards, length of the microstrip line and size of the grounded vias are both tuned to optimize the impedance matching performance. Finally, this prototype is simulated by using the same aforementioned simulator as well, with its optimized dimensions given in Fig. 7.

Experimental results and discussions

The two designed prototypes are fabricated by using the standard PCB process. A Rogers RT/duroid 6002 substrate with the same parameters in Section "SIW power dividing/combing unit cell" is utilized for fabrication. After fabrication, all five ports of the prototype are soldered with SMA coaxial connectors. Two coaxial terminations are connected to the isolated ports of the first prototype, and two 50 Ω lumped resistors with 0603 assembly form are silver soldered to the second prototype with the silver–copper–zinc composite alloys. The measurement is carried out by using an Agilent E8363C vector network analyzer, with the default short-open-load-thru calibration is utilized to remove the influence from the coaxial cables. The thru-reflect-line (TRL) calibration is not used since the three-port TRL calibration is much more complex than the two-port case, therefore, the influence of the SMA connectors on the phase and amplitude balance and insertion losses is unable to be removed. Figure 8 shows the simulated and measured results of the prototype with coaxial terminations, with the photograph shown in the inset. As shown in Fig. 8(a), input and output return losses of the fabricated power combiner/divider with coaxial terminations are both over 10.5 dB. Meanwhile, its insertion losses are about 4.5 ± 0.5 dB, and the isolation is better than 17.5 dB from 13.8 to 19.5 GHz, corresponding to FBW of 33%, as shown in Fig. 8(b). Moreover, it can also be obtained from Fig. 8(c) that the measured amplitude imbalance is less than ±0.4 dB and the measured phase imbalance is less than ±2.5°.

On the other hand, a comparison between the simulated and measured results of the fabricated prototype with lumped resistors is shown in Fig. 9, as well as its photograph. According to

https://doi.org/10.1017/S1759078718000995 Published online by Cambridge University Press

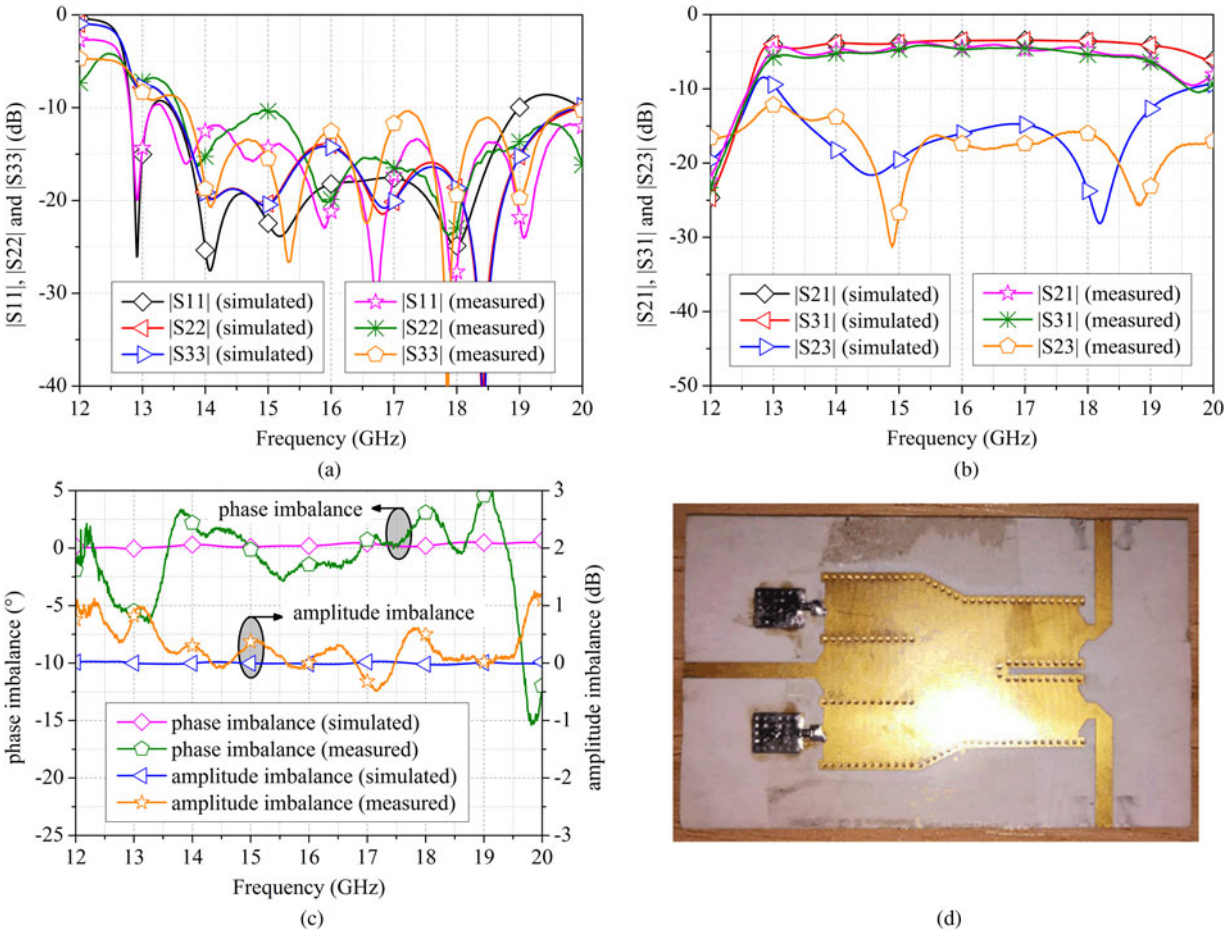


Fig. 9. Simulated and measured results of the fabricated SIW power divider/combiner with lumped resistors. (a) Input and output return losses; (b) insertion losses and isolation; (c) phase and amplitude imbalances; (d) photograph of the fabricated prototype.

Table 1. Comparison between some reported similar SIW power dividers and the presented works

Ref.	f_c (GHz), FBW (isolation > 16 dB)	Insertion loss (dB)	Amplitude imbalance (dB)	Phase imbalance (°)
[3]	11.5, 30%	3.5–5.1	±0.5	±2.5
[5][a]	14.5, 28%	6.4 ± 0.45	±0.5	>10
[6]	20.35, 16%	4.0 ± 0.6	0.3–1	/
Ours-1	16.5, 35%	4.5 ± 0.5	±0.4	±2.5
Ours-2	16.0, 25%	4.8 ± 0.5	±0.5	±3.0

[a]Results of the three-way power divider.

Fig. 9(a), the measured input return loss of the fabricated SIW power divider/combiner with lumped resistors is better than 13 dB, and the output ones are over 10 dB. Moreover, from Fig. 9(b), the measured isolation is over 16 dB from 14.5 to 19 GHz, and the insertion losses are about 4.8 ± 0.5 dB from 14 to 18 GHz, corresponding to an FBW of 25%. Meanwhile, the measured amplitude and phase imbalances are about ±0.5 dB and less than ±3°, respectively, which are given in Fig. 9(c).

Table 1 summarizes the comparison between some reported similar SIW power dividers and the presented ones. Compared with the two-way power divider in [3], the presented ones are with lower amplitude imbalance, with similar insertion loss and phase imbalance. Compared with the three-way power divider in [5], the presented ones are with better amplitude and phase balance performance. Even though the power divider in [6] is with lower insertion loss and similar amplitude imbalance, its FBW is much narrower, and its thick film fabrication is expensive and complex. Based on all the comparison mentioned above, the proposed SIW power dividers/combiners achieve a good trade-off between bandwidth, isolation, insertion loss, phase, and amplitude imbalances. Moreover, the five-port power dividing/combining unit cell has provided a new building-block to set up waveguide power dividers.

https://doi.org/10.1017/S1759078718000995 Published online by Cambridge University Press

Conclusion

Two 3 dB H-plane wideband high-isolated SIW power combiners/dividers with well-balanced performance are developed. A 17.5 dB-isolation FBW of 33% and a 16 dB-isolation FBW of 25% are achieved by the two prototypes, respectively, as well as good phase and amplitude balances. Compared with some reported works realized in the same technology, the proposed one with coaxial termination exhibits a wider bandwidth for the same isolation performance, as well as similar insertion loss, phase, and amplitude balance. The proposed one with lumped resistors also shows a similar performance as the references. Therefore, the proposed SIW power dividers/combiners are promising to be utilized in the wideband phased array antennas and power-combining amplifiers applications in the future wireless communication and radar systems.

Acknowledgements. This work was supported in part by the National Science and Technology Major Project under grant no. 2016ZX03001022-004, the National Science Foundation of China under grant no. 61601087, and the Fundamental Research Funds for Central Universities under grant no. ZYGX2016004.

References

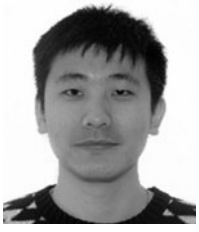
1. **Deslandes D and Wu K** (2001) Integrated microstrip and rectangular waveguide in planar form. *IEEE Microwave and Wireless Components Letters* **51**, 68–70.
2. **Zhang Z-Y and Wu K** (2008) Broadband half-mode substrate integrated waveguide (HMSIW) Wilkinson power divider. *IEEE MTT-S International Microwave Symposium Digest* **51**, 879–882.
3. **Smith NA and Abhari R** (2010) Compact substrate integrated waveguide Wilkinson power dividers. *Proceedings of the IEEE Antennas and Propagation Society International Symposium*, pp. 1–4.
4. **Kazemi R and Fathy AE** (2015) Design of a wideband eight-way single ridge substrate integrated waveguide power divider. *IET Microwaves & Antennas Propagation* **9**, 648–656.
5. **Liu Z and Xiao GB** (2014) New multi-way SIW power dividers with high isolation. *Proceedings of the Asia-Pacific Microwave Conference*, pp. 1–4.
6. **Rave C and Jacob AF** (2015) A multilayer substrate integrated 3 dB power divider with embedded thick film resistor. *Proceedings of the European Microwave Conference*, pp. 482–485.
7. **Pasian M, Silvestri L, Rave C, Bozzi M, Perregrini L, Jacob AF and Samanta KK** (2017) Substrate-integrated-waveguide E-plane 3-dB power-divider/combiner based on resistive layers. *IEEE Transactions on Microwave Theory and Techniques* **65**, 1498–1510.
8. **Alessandri F, Giordano M, Guglielmi M, Martirano G and Vitulli N** (2003) A new multiple-tuned six-port Riblet-type directional coupler in rectangular waveguide. *IEEE Transactions on Microwave Theory and Techniques* **51**, 1441–1448.
9. **Auld BA** (1959) The synthesis of symmetrical waveguide circulators. *IRE Transactions on Microwave Theory Techniques* **7**, 238–243.
10. **Ding J, Wang Q, Zhang Y and Wang C** (2014) A novel five-port waveguide power divider. *IEEE Microwave and Wireless Components Letters* **24**, 224–226.
11. **Huang YM, Jiang W, Jin H, Zhou Y, Leng S, Wang G and Wu K** (2017) Substrate-integrated waveguide power combiner/divider incorporating absorbing material. *IEEE Microwave and Wireless Components Letters* **27**, 885–887.
12. **Pozar DM** (2011) *Microwave Engineering*, 4th Edn. New York: Wiley.
13. **Collin RE** (1992) *Foundations for Microwave Engineering*, 2nd Edn. New York: McGraw-Hill.



Yong Mao Huang received the B.S. degree in Communication Engineering and a Ph.D. degree in Communication and Information Systems from the University of Electronic Science and Technology of China (UESTC), Chengdu, China, in 2010 and 2017, respectively. From 2014 to 2015, he was with the Department of Electrical Engineering, University of South Carolina, Columbia, SC, USA. Since 2018, he has been an Assistant Professor at the School of Electrical and Electronic Information, Xihua University, Chengdu, China. His research interests include radiofrequency/microwave/millimeter-wave circuits and systems for wireless communication, radar and sensing applications, substrate-integrated circuits and antennas, and reconfigurable components. He has authored and coauthored over 40 referred papers. He serves as a reviewer for various IEEE, IET and ACES journals, transactions and letters. He has served as the Technical Program Committee Member of the 2018 IEEE MTT-S International Conference on Microwaves in Mobility (ICMIM 2018) in Munich, Germany, and several other international conferences/symposia.



Haiyan Jin received the B.S. degree in Electronic Information Technology, M.S. and Ph.D. degrees in Electrical Engineering from the University of Electronic Science and Technology of China in 2001, 2006 and 2010, respectively. From 2013 to 2014, he was a postdoc at the Poly-Grames Research Center, École Polytechnique de Montreal, University of Montreal, Montreal, QC, Canada, where he focused on the beam-forming antennas. Since 2010, he has been at the School of Information and Communication Engineering, University of Electronic Science and Technology of China (UESTC), Chengdu, China, where he is now Associate Professor. His current research interests include the antenna array designs and substrate-integrated techniques for microwave and millimeter-wave communication systems. He has authored or coauthored over 70 referred papers. He is a reviewer of several IEEE and IET journals, transactions and letters. He has also served as Technical Program Committee members and Session Chairs for various international conferences.



Yuliang Zhou received the B.S. degree in Applied Physics from the University of Electronic Science and Technology of China, Chengdu, China, in 2012, where he is currently pursuing Ph.D. degree. Since September 2017, he has been with the Microwave Laboratory, Department of Electrical, Computers and Biomedical Engineering, University of Pavia, Pavia, Italy as a visiting Ph.D. student. His current research interests include substrate-integrated circuits, leaky-wave antennas, hybrid oscillators and resonance-based sensing systems. He has authored over 10 publications in referred journals and international conferences/symposia. He has served as a reviewer for several peer-reviewed periodicals and international conferences/symposia.



Supeng Leng received the Ph.D. degree from Nanyang Technological University (NTU), Singapore. He was a Research Fellow of the Network Technology Research Center, NTU. He is currently a Professor and Vice Dean of the School of Information and Communication Engineering, University of Electronic Science and Technology of China, Chengdu, China. His current research interests include resource, spectrum, energy, routing and networking in the Internet

https://doi.org/10.1017/S1759078718000995 Published online by Cambridge University Press

of Things, vehicular networks, broadband wireless access networks, smart grid, and the next generation mobile networks. He has authored over 150 publications in referred journals and international conferences/symposia. He has served as Organizing Committee Chair, Technical Program Committee Chair/Member for many international conferences, as well as a reviewer for over 10 international peer-reviewed journals.



Maurizio Bozzi received the Ph.D. degree from the University of Pavia (Italy) in 2000. He held research positions with various universities worldwide, including Technische Universität Darmstadt (Germany), Universitat de Valencia (Spain), École Polytechnique de Montréal (Canada) and Tianjin University (China). He is currently an Associate Professor at the University of Pavia. His main research interests include computational electromagnetics, substrate-integrated waveguide technology, and novel materials and fabrication technologies for microwave circuits (including paper, textile, and 3D printing). He is a Fellow of the IEEE. He is an Elected Member of the Administrative Committee of the IEEE Microwave Theory and Techniques Society and was a Member of the General Assembly of the European Microwave Association. He is an associate editor for IEEE Microwave and Wireless Components Letters, Electronics Letters, and IET Microwaves, Antennas and Propagation. He was the General Chair of IEEE IMWS-AMP 2017, IEEE NEMO 2014, and IEEE IMWS-MWIT 2011.

https://doi.org/10.1017/S1759078718000995 Published online by Cambridge University Press